ER network formation and membrane fusion by atlastin1/SPG3A disease variants

Idil Ulengin, John J. Park and Tina H. Lee
Department of Biological Sciences, Carnegie Mellon University, Pittsburgh, PA 15213

ABSTRACT **At least 38 distinct missense mutations in the neuronal atlastin1/SPG3A GTPase are implicated in an autosomal dominant form of hereditary spastic paraplegia (HSP), a motor-neurological disorder manifested by lower limb weakness and spasticity and length-dependent axonopathy of corticospinal motor neurons. Because the atlastin GTPase is sufficient to catalyze membrane fusion and required to form the ER network, at least in nonneuronal cells, it is logically assumed that defects in ER membrane morphogenesis due to impaired fusion activity are the primary drivers of SPG3A-associated HSP. Here we analyzed a subset of established atlastin1/SPG3A disease variants using cell-based assays for atlastin-mediated ER network formation and biochemical assays for atlastin-catalyzed GTP hydrolysis, dimer formation, and membrane fusion. As anticipated, some variants exhibited clear deficits. Surprisingly however, at least two disease variants, one of which represents that most frequently identified in SPG3A HSP patients, displayed wild-type levels of activity in all assays. The same variants were also capable of co-redistributing ER-localized REEP1, a recently identified function of atlastins that requires its catalytic activity. Taken together, these findings indicate that a deficit in the membrane fusion activity of atlastin1 may be a key contributor, but is not required, for HSP causation.**

Monitoring Editor
Benjamin S. Glick
University of Chicago

Received: Oct 14, 2014
Revised: Mar 2, 2015
Accepted: Mar 3, 2015

INTRODUCTION

Hereditary spastic paraplegia (HSP) is an uncommon but not rare disorder (afflicting ~3–9/100,000 individuals) that causes weakness and spasticity in the lower limbs of affected individuals while largely sparing the upper extremities (Fink, 2006; Depienne *et al.*, 2007; Salinas *et al.*, 2008; Blackstone, 2012). Postmortem analysis of HSP patients revealed a length-dependent degeneration of the longest axons in the corticospinal tract (Deluca *et al.*, 2004). More than 55 distinct spastic paraplegia genes (SPGs) have been identified (Lo Giudice *et al.*, 2014), and the products can be grouped into functions having to do with axon path finding, myelination, receptor trafficking, organelle movement, mitochondrial function, and endoplasmic reticulum (ER) morphogenesis (Blackstone *et al.*, 2011). Consequently, a deficit in one or more cellular pathways necessary for long-axon maintenance has been proposed to underlie the symptoms of HSP (Blackstone, 2012).

The original identification of atlastin1/SPG3A occurred through genetic analysis of three independent kindreds (autosomal dominant [AD] HSP-P, -T, and -S), each presenting with an early-onset autosomal dominant form of HSP (Zhao *et al.*, 2001). In each case, the disease segregated with a single genetic locus termed SPG3A (Hazan *et al.*, 1993; Gispert *et al.*, 1995), which was ultimately narrowed to a 2.7-cM region on chromosome 14 (Rainier *et al.*, 2001). Sequencing the open reading frames within the mapped region uncovered a point mutation in the atlastin1 gene in all three kindreds (Zhao *et al.*, 2001). Each kindred had a distinct mutation, but within each kindred, the affected members were invariably positive for the same mutation at one of two alleles. None of the asymptomatic individuals had the mutation, indicating a high degree of penetrance (Zhao *et al.*, 2001). Since its original identification, >30 additional atlastin1/SPG3A mutations, mostly missense mutations within the GTPase domain, have been identified in early-onset HSP patients (Guelly *et al.*, 2011).

This article was published online ahead of print in MBoC in Press (http://www.molbiolcell.org/cgi/doi/10.1091/mbc.E14-10-1447) on March 11, 2015.

Address correspondence to: Tina H. Lee (thl@andrew.cmu.edu).

Abbreviations used: ADHSP, autosomal dominant hereditary spastic paraplegia; BMOE, bismaleimidoethane; 3HB, three-helix bundle; HSP, hereditary spastic paraplegia; SPG, spastic paraplegia gene.

© 2015 Ulengin *et al.* This article is distributed by The American Society for Cell Biology under license from the author(s). Two months after publication it is available to the public under an Attribution–Noncommercial–Share Alike 3.0 Unported Creative Commons License (http://creativecommons.org/licenses/by-nc-sa/3.0).
"ASCB®," "The American Society for Cell Biology®," and "Molecular Biology of the Cell®" are registered trademarks of The American Society for Cell Biology.

Atlastin1/SPG3A expression in vertebrates is enriched in the CNS (Zhao *et al.*, 2001; Zhu *et al.*, 2006). Accordingly, the first studies aimed at elucidating function used a neuronal cell culture model in which silencing of atlastin1 impaired axonal outgrowth (Zhu *et al.*, 2006). Concurrent studies showed overexpression of an atlastin1/SPG3A mutant variant, localized to the ER in HeLa cells, perturbing ER network morphology in a dominant-negative manner, suggesting a possible role in ER morphogenesis (Rismanchi *et al.*, 2008). In support, siRNA-mediated depletion of the more ubiquitously expressed atlastin2 and atlastin3 isoforms also caused ER morphological abnormalities (Hu *et al.*, 2009). Collectively the data suggested a role for the atlastins in ER network morphogenesis.

Precisely how atlastins mediate ER morphogenesis remains to be elucidated. The similarity of the GTPase domain of atlastin to that of dynamins and mitofusins, mechanochemical enzymes that mediate membrane fission and fusion, respectively (Praefcke and McMahon, 2004), led investigators early on to hypothesize a direct membrane-remodeling role (Rismanchi *et al.*, 2008). Soon thereafter, purified *Drosophila melanogaster* atlastin was demonstrated to be sufficient to catalyze lipid bilayer fusion when incorporated into synthetic lipid vesicles (Orso *et al.*, 2009). Fusion was GTP hydrolysis dependent, prompting the idea that atlastin might represent the long-sought GTP-dependent fusion machinery for the ER (Dreier, 2000). It is now known that atlastin, similar to dynamin (Chappie *et al.*, 2010), and other GTPases that undergo nucleotide-dependent head-to-head dimerization (Gasper *et al.*, 2009), forms a transhomodimer as it catalyzes GTP hydrolysis (Byrnes *et al.*, 2013). Transdimerization in atlastin is further accompanied by a rigid-body rotation of a three-helix bundle (3HB) connecting each GTPase head domain to its membrane anchor. This rotation causes the 3HBs to cross over one another and is proposed to bring the 3HBs, pointing away from the dimer interface and anchored in opposing membranes initially, into close parallel alignment such that they come to reside within the same membrane (Bian *et al.*, 2011; Byrnes and Sondermann, 2011). Crossover is hypothesized to constitute the driving force for membrane fusion (Daumke and Praefcke, 2011).

The long-axon degeneration associated with SPG3A-linked HSP could be explained simply by the inability of atlastin1/SPG3A disease variants to catalyze ER membrane fusion and network formation. Although compelling, a clear demonstration of this hypothesis has remained elusive. In particular, the idea that a reduction in the membrane fusion activity of atlastin1/SPG3A causes HSP lacks strong support. This may be due in part to the lack of an ideal assay system: whereas the *Drosophila* orthologue (Orso *et al.*, 2009) and, more recently, other atlastin counterparts in more distantly related organisms (Anwar *et al.*, 2012; Zhang *et al.*, 2013) have been shown to catalyze the fusion of synthetic membranes, the human proteins have not yet been demonstrated to possess this activity, for unknown reasons (Wu *et al.*, 2015). Consequently, assessment of the fusion capability of atlastin1/SPG3A mutant variants has relied on transfer of point mutations to the *Drosophila* orthologue, and only a few have been analyzed in this manner (Bian *et al.*, 2011). In addition, a large number of truncated atlastin1/SPG3A mutant variants were analyzed in the soluble phase for their ability to hydrolyze GTP and dimerize in a nucleotide-dependent manner (Byrnes and Sondermann, 2011). Surprisingly, no clear correlation between disease-causing mutations and biochemical activity emerged from that analysis. For many variants, the impairment of GTP hydrolysis and dimer formation was modest at best (Byrnes and Sondermann, 2011).

The idea that SPG3A HSP is caused by ER morphology defects similarly lacks strong support. Simply put, the status of the ER in neurons expressing the SPG3A disease mutations remains unknown. This is due in part to the lack of an appropriate animal model for the disease. It may also be due to the peculiarities of neuronal cell shape, which make the details of the branched tubular ER network a challenge to image (Dailey and Bridgman, 1989; Terasaki *et al.*, 1994). In any case, further investigation is needed to determine whether atlastin1/SPG3A mutations invariably perturb ER network structure.

Our lab previously established a functional replacement assay that demonstrated the capacity of an exogenously introduced non-neuronal atlastin2 to mediate ER network formation in HeLa cells depleted of endogenous atlastins (Morin-Leisk *et al.*, 2011). We recently showed that *Drosophila* atlastin was also capable of functionally replacing human atlastins in this system (Faust *et al.*, 2015). Because *Drosophila* atlastin can catalyze membrane fusion in a robust manner (Orso *et al.*, 2009) and shares 66% amino acid identity with atlastin1 in its GTPase domain, we reasoned that analysis of the atlastin1/SPG3A mutations transferred to the *Drosophila* orthologue afforded a unique opportunity to assess simultaneously individual atlastin1/SPG3A mutations for their effects on both ER morphogenesis and membrane fusion catalysis. On the basis of current thinking in the field, we started with the hypothesis that each atlastin1/SPG3A mutant variant would exhibit a measurable deficit both in its ability to mediate network formation and in its ability to catalyze membrane fusion. Surprisingly, our results indicated that although this was the case for some of the variants, it was not the case for others. In particular, two of the three mutations (in the ADHSP-T and -S kindreds) that led to the original identification of atlastin1/SPG3A (Zhao *et al.*, 2001) caused no measurable deficit in any assay. Our findings lead us to question whether impaired ER membrane fusion is the sole driver of SPG3A HSP.

RESULTS

Atlastin1/SPG3A mutations

Atlastins consist of a large, globular, cytoplasmic GTPase domain followed by a 3HB, which is in turn anchored to ER membranes by a pair of transmembrane helices and a cytoplasmic tail (Rismanchi *et al.*, 2008; Bian *et al.*, 2011; Byrnes and Sondermann, 2011). Figure 1 shows the identity and location of the 38 distinct atlastin1/SPG3A mutations identified at the time of a recent report (Guelly *et al.*, 2011) and further updated on the Human Gene Mutation Database (www.hgmd.cf.ac.uk/ac/search.php). A number of variants were previously produced in truncated form and analyzed in the soluble phase (Byrnes and Sondermann, 2011). Some were insoluble when expressed in *Escherichia coli*, consistent with protein folding or stability issues (Figure 1; underlined mutations; Byrnes and Sondermann, 2011); others, including R217Q and Q191R, were stably expressed but strongly defective in dimerization and/or GTP hydrolysis (Byrnes and Sondermann, 2011). The basis for disease causation for those variants seemed clear. It is of interest, however, that a substantial number of the remaining variants showed only modest impairment (Byrnes and Sondermann, 2011). To understand better the basis for disease for these mildly impaired variants, we set out to analyze them using broader functional assays encompassing ER network formation and membrane fusion catalysis.

Not all SPG3A/atlastin1 mutations impair ER network formation

To assess ER network formation, we used HeLa cells because their relatively flat shape makes imaging of the branched tubular morphology of the ER network straightforward. As previously reported

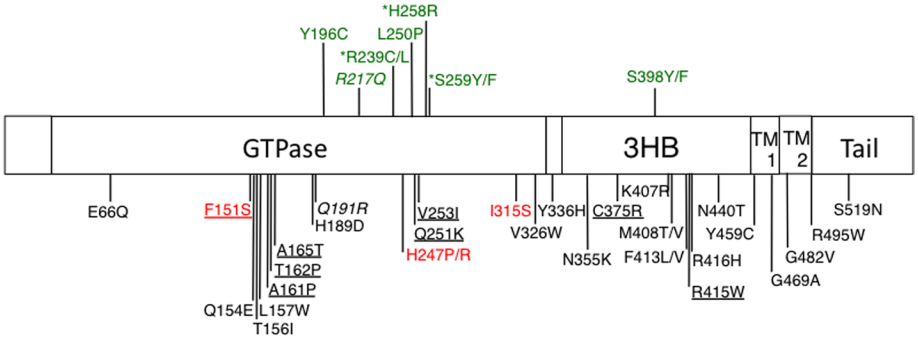

FIGURE 1: Atlastin1/SPG3A mutations. The positions of known atlastin1/SPG3A mutations as of a recent report (Guelly *et al.*, 2011) and further updated (www.hgmd.cf.ac.uk/ac/search.php) are indicated on an atlastin1 primary sequence map. Mutations that caused insolubility when expressed in the context of the atlastin1 soluble domain are underlined (Byrnes *et al.*, 2011); mutations that greatly reduced GTPase activity or dimer formation are italicized; mutations that inhibited fusion activity when transferred to *Drosophila* atlastin are in red (Bian *et al.*, 2011); mutations occurring in the families ADHSP-P, ADHSP-T, and ADHSP-S are indicated by an asterisk (Zhao *et al.*, 2001), and the mutations analyzed in this study are in green.

(Hu *et al.*, 2009; Morin-Leisk *et al.*, 2011), RNA interference (RNAi)–mediated atlastin2/3 knockdown perturbed the ER in HeLa. Whereas the ER in nearly all control cells consisted of a densely branched network of polygons (Figure 2, A and inset; quantified in Figure 2, E and F), ER tubules ran largely parallel to one another in 57% of knockdown cells, and there was a significant reduction in three-way junctions in those cells (Figure 2, B and inset; quantified in Figure 2, E and F). Expression of either enhanced yellow fluorescent protein (eYFP)–tagged *Drosophila* atlastin (Figure 2, C and inset; quantified in Figure 2, E and F) or hemagglutinin (HA)-tagged atlastin1 (Figure 2, D and inset; quantified in Figure 2, E and F), maintained normal network branch point density after endogenous atlastin depletion,

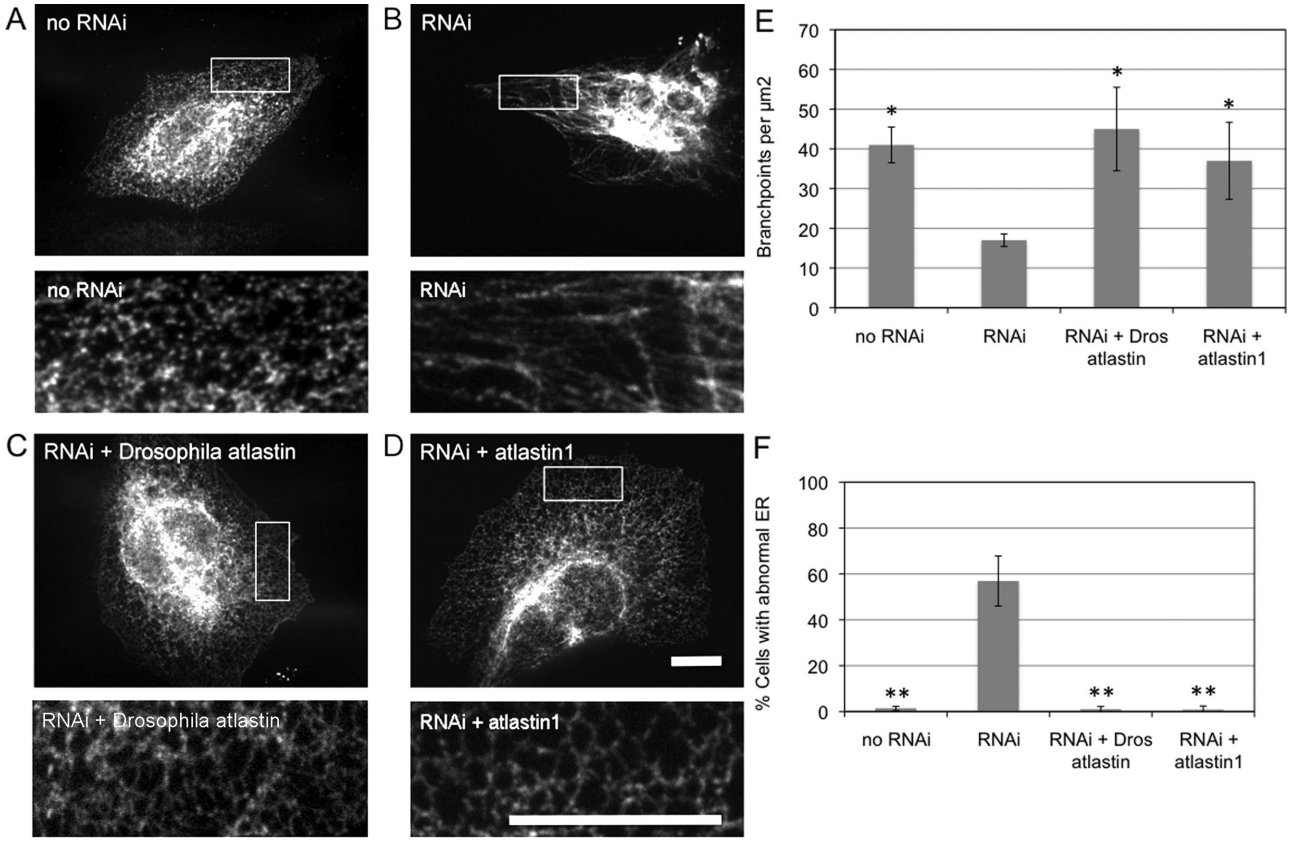

FIGURE 2: Atlastin1 and *Drosophila* atlastin maintain a normal branched ER network in HeLa cells in the absence of atlastin2/3. At 48 h after transfection with Myc-tagged REEP5/DP1/TB2 (neg con; A, B), eYFP-tagged *Drosophila* atlastin (C), or HA-tagged atlastin1 (D), cells were either left untreated (A) or further transfected using siRNAs targeting atlastin2/3 (B–D). At 72 h after knockdown, cells were fixed and stained using an antibody against the Myc or HA epitope and viewed by confocal microscopy. Scale bars, 10 µm. The insets in A–D show magnified views of a boxed region of the peripheral ER. (E) Quantification of the average number of network branch points (±SD) in five representative 100-µm^2 boxed peripheral regions of the ER under each condition. (F) Quantification of the percentage of cells expressing Myc-REEP5/DP1/TB2 (with or without RNAi), eYFP–*Drosophila* atlastin (with RNAi), or HA-atlastin1 (with RNAi) that displayed an abnormal unbranched ER morphology. Values represent the means of three independent experiments (>100 cells each) ± SD. *$p < 0.001$ and **$p < 0.0001$ (unpaired Student's *t* test) relative to the RNAi-treated negative control.

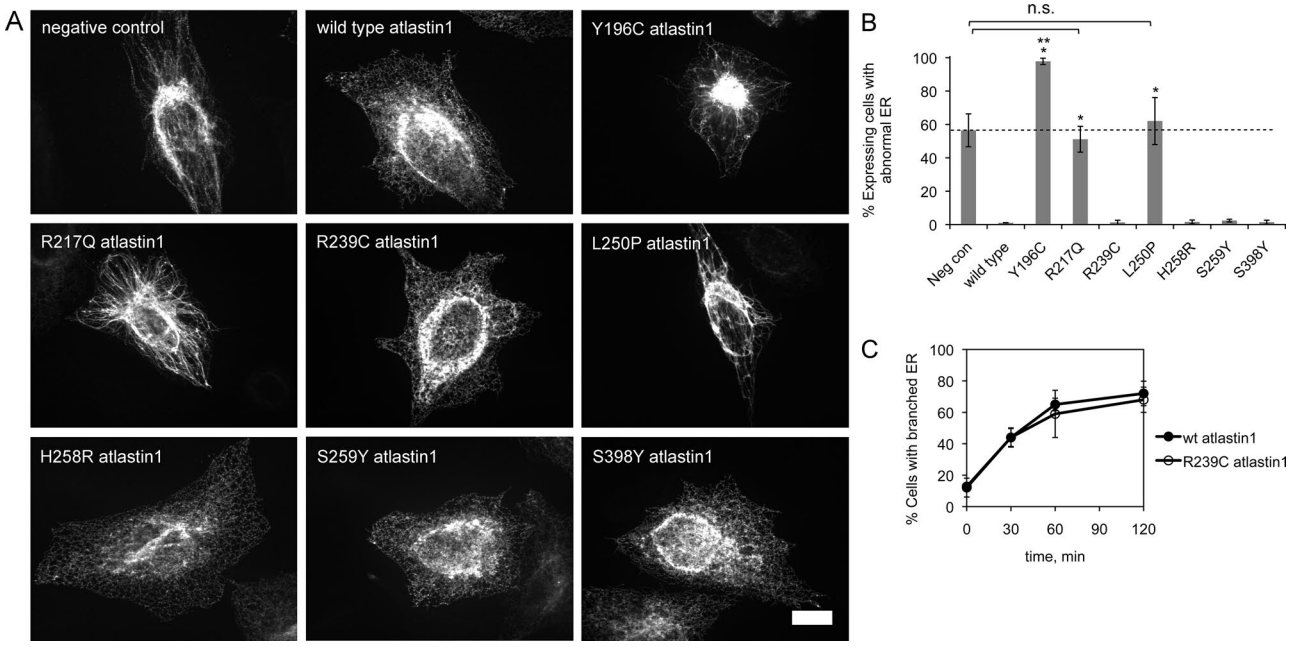

FIGURE 3: Some but not all atlastin1/SPG3A variants are defective in forming a branched ER network. (A) At 48 h after transfection with the indicated HA-tagged atlastin1 variant constructs, HeLa cells were further transfected using siRNAs targeting endogenous atlastin2/3. At 72 h after knockdown, cells were fixed and stained using an antibody against the HA epitope and viewed by confocal microscopy. The negative control was Myc-tagged REEP5/DP1/TB2 stained with an antibody against the Myc epitope. Scale bar, 10 μm. (B) Quantification of the percentage of cells expressing the HA- or Myc-tagged construct and showing an abnormal unbranched ER morphology. Values represent the means of three independent experiments (>100 cells each) ± SD. *$p < 0.0001$ with respect to the wild type and **$p < 0.0001$ with respect to the negative control. R217Q and L250P were not significantly different from the negative control (unpaired Student's *t* test). (C) Quantification of de novo branched ER network formation. After knockdown and replacement with either HA-tagged wild-type or R239C atlastin1 as in A, cells were treated for 3 h with nocodazole to induce microtubule depolymerization and ER collapse, followed by drug washout. At the indicated times, cells were fixed and stained with antibodies against HA and tubulin (Supplemental Figure S2). The percentage of cells expressing the HA-tagged construct and displaying a normal branched ER morphology was quantified. Values represent the means of three independent experiments (>100 cells each) ± SD.

and the percentage of cells with an unbranched ER phenotype fell from 57% to 1 or 0.8% of expressing eYFP-*Drosophila* atlastin or HA-atlastin1, respectively. To monitor ER morphology in untreated and control RNAi-treated cells (Figure 2, A and B), we used a Myc-tagged version of the tubular ER marker REEP5/DP1/TB2 (Hashimoto *et al.*, 2014), which by itself had no discernible effect on ER morphology in either control or knockdown cells (Morin-Leisk *et al.*, 2011). Overall our observations were consistent with recent reports of phenotypic rescue of RNAi-induced ER defects by *Drosophila* atlastin in HeLa (Faust *et al.*, 2015) and by atlastin1 and *Drosophila* atlastin in Cos-7 cells (Wu *et al.*, 2015). The similarity of morphological rescue by these distinct atlastins underscored the conservation of atlastin function in ER network morphogenesis.

We next assessed individual atlastin1/SPG3A mutant variants that previously showed only modest impairment in soluble-phase assays (Figure 1, highlighted in green). As a control, we included R217Q, which is reported to lack both GTP hydrolysis and dimerization ability due to mutation of a key GTP-binding residue (Rismanchi *et al.*, 2008; Byrnes and Sondermann, 2011). As anticipated, the R217Q atlastin1 variant was unable to maintain a branched ER network, similar to the negative control (Figure 3A; quantified in Figure 3B). Lack of function was also observed for Y196C and L250P atlastin1 (Figure 3A; quantified in Figure 3B). Y196C atlastin1 exerted such a strong dominant-negative effect that it further increased the fraction of knockdown cells with abnormal ER morphology, from 57% in the control to 98% (Figure 3B). It is likely that this variant perturbed ER network formation even in cells with only partial atlastin2/3 knockdown. Costaining for the tubular ER marker REEP5/DP1/TB2 indicated that all three nonfunctional variants retained ER localization (Supplemental Figure S1). In sum, even though Y196C and L250P showed only modest deficits when analyzed in the soluble phase (Byrnes and Sondermann, 2011), they exhibited strong defects in our functional replacement assay. Surprisingly, however, and in clear contrast, several atlastin1/SPG3A variants scored as well as the wild type (Figure 3A; quantified in Figure 3B). Of note, these functional variants included R239C, H258R, and S259Y atlastin1, corresponding to the ADHSP-S, ADHSP-T, and ADHSP-P familial mutations that originally led to the identification of atlastin1/SPG3A.

We wondered whether the apparent functionality of these prominent disease variants might be due to the order of manipulations in our replacement assay. Given that expression of the test atlastin1 variant was typically induced before RNAi treatment, it was possible that these "functional" variants might be capable of sustaining an ER network already established before knockdown but incapable of mediating network formation de novo. To address this possibility, we carried out a nocodazole-washout regime. Nocodazole treatment abolishes the microtubule tracks upon which ER membranes extend (Waterman-Storer, 1998; Friedman *et al.*, 2010), thereby inducing a near-complete retraction of the ER toward the cell center

and loss of the peripheral tubular network (Terasaki *et al.*, 1986; Lu *et al.*, 2009). On drug washout, microtubule reassembly provides new tracks for ER network reformation (Terasaki *et al.*, 1986). As shown (Supplemental Figure S2) and quantified (Figure 3C), there was no significant difference in reestablishing an ER network between cells rescued with wild-type or R239C atlastin1. The percentage of cells displaying a branched tubular ER network decreased in dramatic manner after nocodazole treatment, from 99% to 13% for wild-type and 12% for R239C atlastin1. By 30 min after drug washout, the percentage of cells with branched ER rose to 44% for both wild-type and R239C atlastin1. By 120 min, 72% (±7.8 SD) of wild-type and 68% (±8 SD) of R239C atlastin1 cells displayed network branching (Figure 3C and Supplemental Figure S2), indicating similar and substantial network reformation in both. Therefore R239C atlastin1 and likely the other functional SPG3A variants were capable of supporting de novo ER network formation.

SPG3A/atlastin1 variants that are functional in ER network formation are also functional in co-redistribution of ER-localized REEP1

A recent study suggested a conserved role for atlastins in the formation of large lipid droplets. Atlastin depletion caused a reduction in lipid droplet size in the intestinal cells of *Caenorhabditis elegans*, as well as in the fat bodies of *Drosophila* (Klemm *et al.*, 2013). Conversely, atlastin1 overexpression induced the appearance of large lipid droplet–like structures in Cos-7 cells, although the enlargement required joint overexpression of REEP1, an ER-structuring protein that binds and bundles microtubules (Park *et al.*, 2010; Klemm *et al.*, 2013). In this instance, the atlastin1 and REEP1 were largely redistributed from ER and ER/microtubule structures, respectively, to structures coincident with BODIPY 493/503 staining, an accepted marker of lipid droplets (Listenberger and Brown, 2007). This ability of atlastin1 to co-redistribute REEP1 was not seen with several atlastin1 variants defective for membrane fusion (Klemm *et al.*, 2013), suggesting that both the ER network formation and lipid droplet enlargement functions of atlastins depended on membrane fusion catalysis. Whether the apparent atlastin requirement for lipid droplet enlargement reflected a direct or indirect requirement for atlastin's fusion function remains to be clarified (Klemm *et al.*, 2013). Nevertheless, it seemed reasonable that analysis of disease variants for their functionality in this new assay might reveal deficits not detectable in our ER network formation assay.

As reported previously (Klemm *et al.*, 2013), exogenous atlastin1 localized to the ER when expressed in Cos-7, and exogenous REEP1 accumulated in microtubule-associated ER structures (Supplemental Figure S3). In contrast, coexpression drove both atlastin1 and REEP1 into enlarged lipid droplet like structures similar to those seen previously (Figure 4A; quantified in Figure 4B). Curiously, these structures did not colocalize with the lipid droplet marker BODIPY 493/503 (Supplemental Figure S4). The basis for our inability to detect BODIPY staining in these structures remains to be clarified. It could reflect differences in the ratios and/or levels of atlastin1 and REEP1 used, or it could reflect a difference in the staining procedure. Nevertheless, the R217Q atlastin1 variant was unable to induce co-redistribution of REEP1 (Figure 4, A and B), consistent with the previous report (Klemm *et al.*, 2013). The Y196C and L250P variants had significantly reduced activity in this assay, as anticipated, but still induced some redistribution (Figure 4, A and B). In contrast, both the R239C and H258R atlastin1 variants co-redistributed REEP1 to large structures to an extent indistinguishable from the wild type (Figure 4, A and B).

Select atlastin1/SPG3A mutations do not impair ER network formation by either atlastin1 or *Drosophila* atlastin

Based on the unexpected functionality of certain atlastin1/SPG3A disease variants in ER network formation, as well as in REEP1 co-redistribution, it was imperative that they be characterized in terms of their effects on membrane fusion catalysis. As mentioned, few if any *Drosophila* counterparts of atlastin1/SGP3A variants had been characterized previously. Therefore we set out to analyze the effects of these mutations when transferred to the *Drosophila* orthologue. Our overall plan was to first assess *Drosophila* versions of the variants in ER network formation, then determine their ability to hydrolyze GTP and form crossover dimers, and finally measure their ability to catalyze membrane fusion.

The R239C and S259Y atlastin1 variants were constructed in *Drosophila* atlastin simply by substituting the identical residues in *Drosophila* atlastin, after sequence alignment, to R214C and S234Y, respectively. For H258R and S398Y, where the corresponding residue in *Drosophila* atlastin was similar but not identical, the *Drosophila* residue was converted to that present in the disease variant. When the eYFP-tagged *Drosophila* atlastin variants were tested, one, A373Y (S398Y in atlastin1), was clearly nonfunctional (Figure 5A; quantified in Figure 5B), as would have been expected for its atlastin1 counterpart. However, in contrast to this variant, the three other *Drosophila* atlastin variants (R214C, S233R, and S234Y, corresponding to R239C, H258R, and S259Y in atlastin1) were again indistinguishable from the wild type (Figure 5, A and B). Of note, these were the same variants present in the ADHSP-S, ADHSP-T, and ADHSP-P kindreds, respectively (Zhao *et al.*, 2001).

Atlastin1/SPG3A mutations R239C, H258R, and S259Y do not impair *Drosophila* atlastin GTPase activity

Our results thus far established that, contrary to our initial expectations, three prominent atlastin1/SPG3A variants, whether in the context of atlastin1 or *Drosophila* atlastin, lacked any detectable deficit in cell-based assays. To characterize biochemically the *Drosophila* versions, we first transferred each mutation to the truncated *Drosophila* atlastin soluble domain (amino acids [aa] 1–415) and performed a standard GTPase assay (Orso *et al.*, 2009). As points of reference, we also included two variants that were incompetent for ER network formation: Y171C and A373Y (Y196C and S398Y in atlastin1). Consistent with their lack of ER network formation functionality (Figure 5, A and B), both the Y171C and A373Y variants had reduced GTPase activity (Figure 6A). In contrast, the other three variants were indistinguishable from the wild type (Figure 6A).

Atlastin1/SPG3A mutations R239C, H258R, and S259Y do not impair *Drosophila* atlastin crossover dimer formation

The same soluble domain variants were next subjected to an assay for nucleotide-dependent crossover dimer formation, which is essential for membrane fusion catalysis (Bian *et al.*, 2011; Pendin *et al.*, 2011; Saini *et al.*, 2014). The assay, developed originally in our lab for atlastin2 (Morin-Leisk *et al.*, 2011), relies on the conjugation of two 3HB cysteines to one another by the short (8 Å) spacer-arm sulfhydryl cross-linking reagent bismaleimidoethane (BMOE) when atlastin is in the crossover dimer configuration but not when it is either monomeric or in the extended dimer configuration. Because *Drosophila* atlastin lacked a cysteine at the same position, the corresponding glycine residue was cysteine substituted to generate G343C *Drosophila* atlastin. Prior analysis indicated that the cysteine substitution did not at all impair membrane fusion functionality (Saini *et al.*, 2014). As anticipated and recently reported (Saini *et al.*, 2014), cross-linked wild-type (G343C) crossover dimers

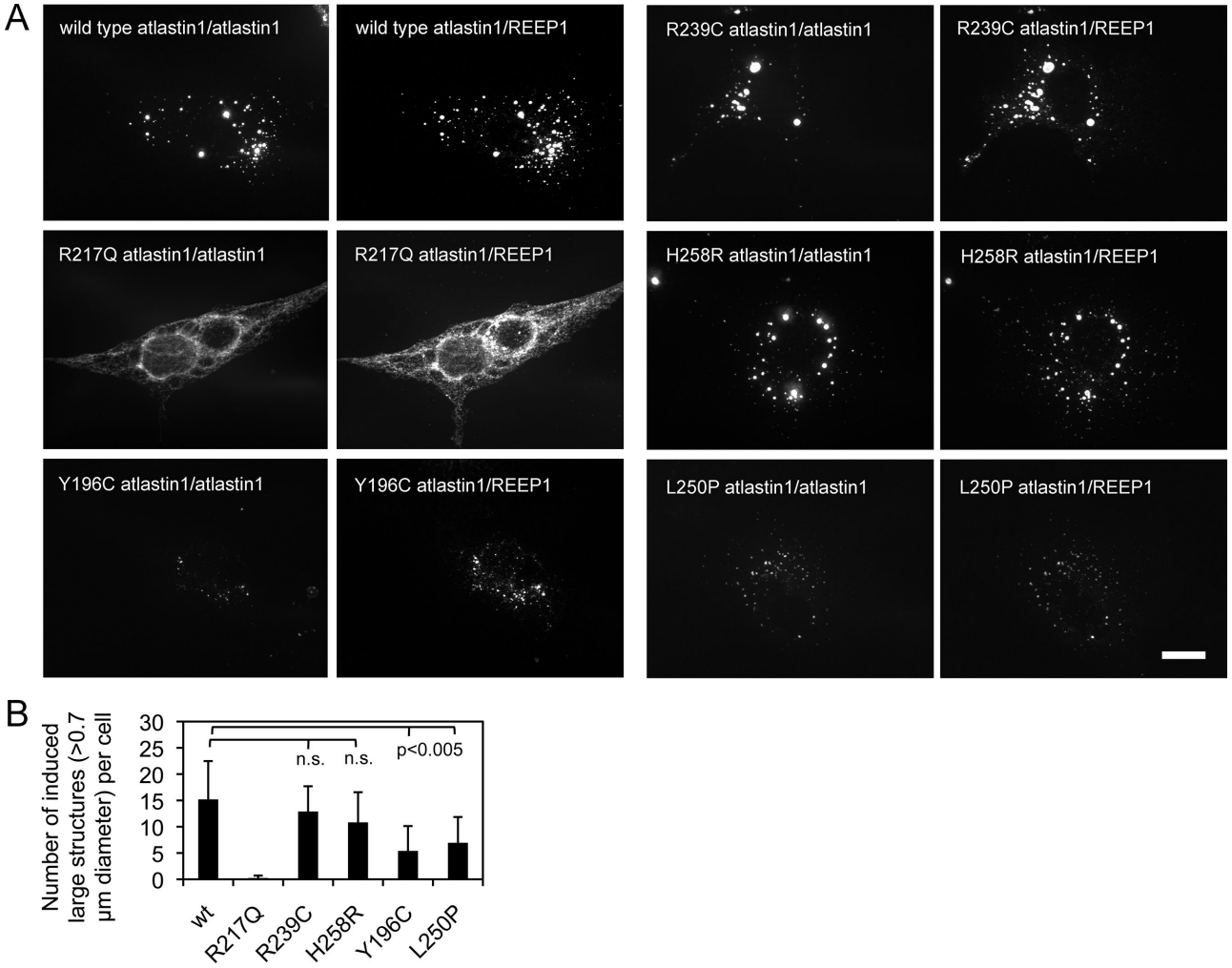

FIGURE 4: Some but not all atlastin1/SPG3A variants are defective in co-redistributing REEP1. (A) The indicated eYFP-atlastin1 and variants were transfected into Cos-7 cells together with Flag-tagged REEP1. At 48 h after transfection, cells were fixed and stained with the Flag epitope antibody and viewed by confocal microscopy. Scale bar, 10 µm. (B) The average number of large structures containing both REEP1 and atlastin1 (>0.7 µm in diameter) per cell ± SD (>10 cells) was quantified in ImageJ. Both the wild type and each of the variants were clearly different from the nucleotide-binding-defective R217Q variant ($p = 0.007$ for L250P and $p < 0.0001$ for all others). Y196C and L250P had reduced activity compared with the wild type ($p < 0.005$), whereas R239C H258R were not significantly different (n.s.) from the wild type ($p = 0.41$ and 0.14, respectively).

were recovered after incubation with GMPPNP, GTP, or GDP-AlF_4^- but not with GDP, AlF_4^- alone, or in the absence of nucleotide (Figure 6B). This behavior largely mirrored that previously observed for atlastin2 (Morin-Leisk *et al.*, 2011). It was also consistent with a fluorescence resonance energy transfer–based stopped-flow kinetic analysis of the atlastin1 soluble domain, showing rapid but transient crossover dimer formation with GTP, slower but irreversible crossover dimer formation with either GMPPNP or GDP-AlF_4^-, and none with GDP or in the absence of nucleotide (Byrnes *et al.*, 2013). Consistent with their reduced GTPase activity (Figure 6A), neither the Y171C nor A373Y variant was captured in the crossover dimer conformation under any nucleotide incubation condition (Figure 6B). Thus each of the variants that showed defects in our cell-based network formation assay (Figure 5, A and B) also had strong defects in crossover dimer formation. In striking contrast, R214C, S233R, and S234Y were each fully capable of forming the crossover dimer and did so in a nucleotide-dependent manner, mirroring that of the wild-type protein (Figure 6B).

Drosophila atlastin variants with R239C, H258R, and S259Y SPG3A-equivalent mutations are fusion competent

The three functional variants were finally expressed in the context of the full-length *Drosophila* protein, purified, incorporated into proteoliposomes, and subjected to an established assay for atlastin-catalyzed membrane fusion (Orso *et al.*, 2009; Bian *et al.*, 2011). Again as a point of reference, we included the Y171C variant (Y196C in atlastin1), which is expected to lack fusion activity due to its inability to mediate ER network formation (Figure 5, A and B), as well as its reduced ability to hydrolyze GTP (Figure 6A) and inability to form crossover dimers (Figure 6B). All variants were purified in similar quantities, indicative of comparable protein stabilities, and incorporated into donor and acceptor vesicles with similar efficiencies (Supplemental Figure S5). As expected (Figure 7), the wild-type protein catalyzed fusion robustly, with similar kinetics and to a similar extent as previously reported (Orso *et al.*, 2009; Bian *et al.*, 2011; Moss *et al.*, 2011). Also as expected, the Y171C variant had no fusion activity (Figure 7). Remarkably however, all three variants,

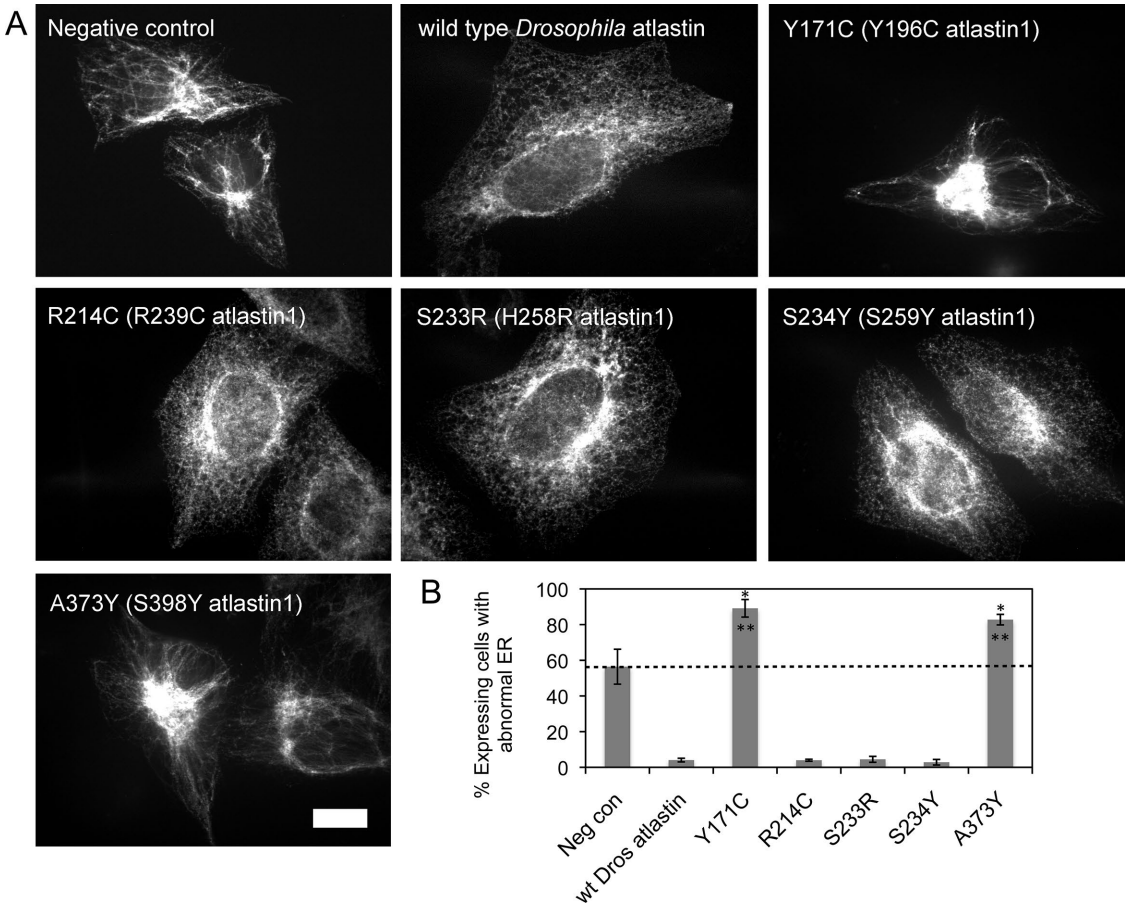

FIGURE 5: Some but not all SPG3A mutations impair ER network formation when expressed in *Drosophila* atlastin. (A) At 48 h after transfection with the indicated eYFP-tagged *Drosophila* atlastin variant constructs, HeLa cells were further transfected using siRNAs targeting endogenous atlastin2 and atlastin3. At 72 h after knockdown, cells were fixed and viewed by confocal microscopy. The negative control Myc-tagged REEP5/DP1/TB2 was stained with an antibody against the Myc epitope. Scale bar, 10 μm. (B) Quantification of the percentage of cells expressing either the Myc-tagged or eYFP-tagged construct and showing an abnormal unbranched ER morphology. Values represent the means of three independent experiments (>100 cells each) ± SD. *$p < 0.0001$ with respect to the wild type and **$p < 0.004$ with respect to the negative control (unpaired Student's *t* test).

R214C, S233R, and S234Y (R239C, H258R, and S259Y in atlastin1), were clearly competent for fusion catalysis. S234Y appeared slightly less active, but both R214C and S233R appeared indistinguishable from the wild type (Figure 7). To obtain a more quantitative comparison of the activities of R214C and S233R relative to wild type, we monitored fusion at a lower protein-to-lipid ratio (1:1000), at which the efficiency of incorporation into donor and acceptor vesicles was again similar between variants (Supplemental Figure S6). As expected, the lower protein-to-lipid ratio resulted in slightly slower and less efficient fusion for the wild-type protein (Figure 8). Even under these conditions, however, both R214C and S233R were at least as active as the wild type in their ability to catalyze membrane fusion (Figure 8). In sum, neither disease variant could be distinguished from the wild type in any of our assays for atlastin functionality.

DISCUSSION

Our study uncovered two distinct categories of atlastin1/SPG3A mutations. Disease mutations of the first category impaired activity in functional assays for ER network formation, REEP1 co-redistribution, and membrane fusion catalysis, although they were reported to reduce activity only modestly in soluble-phase biochemical assays (Byrnes and Sondermann, 2011). In contrast, little or no effect on ER network formation, REEP1 co-redistribution, or membrane fusion catalysis could be detected for disease mutations of the second category. The behavior of the first group was anticipated and consistent with perturbation of the ER network as the root cause of the disease. The behavior of the second group was entirely unexpected. Overall our findings reveal a notable gap in understanding of how atlastin function and dysfunction contributes to health and disease.

The Y196C, L250P, and S398Y atlastin1/SPG3A mutations impaired activity in multiple assays. The precise structure–function relationship of each of these mutations remains to be understood. Y196C and S398Y strongly inhibited GTP-dependent crossover dimer formation when transferred to the *Drosophila* soluble domain. For these mutations, inspection of the atlastin1 crystal structures reveals potential explanations for functional perturbation. For instance, the side chain of Y196, a residue within the globular GTPase head, contacts a residue outside the head specifically in the crossover dimer configuration (Bian *et al.*, 2011; Byrnes and Sondermann, 2011). The residue that it contacts, P342, resides within the linker connecting the head to the 3HB and constitutes the pivot point of 3HB rotation (Bian *et al.*, 2011; Byrnes and Sondermann, 2011). On

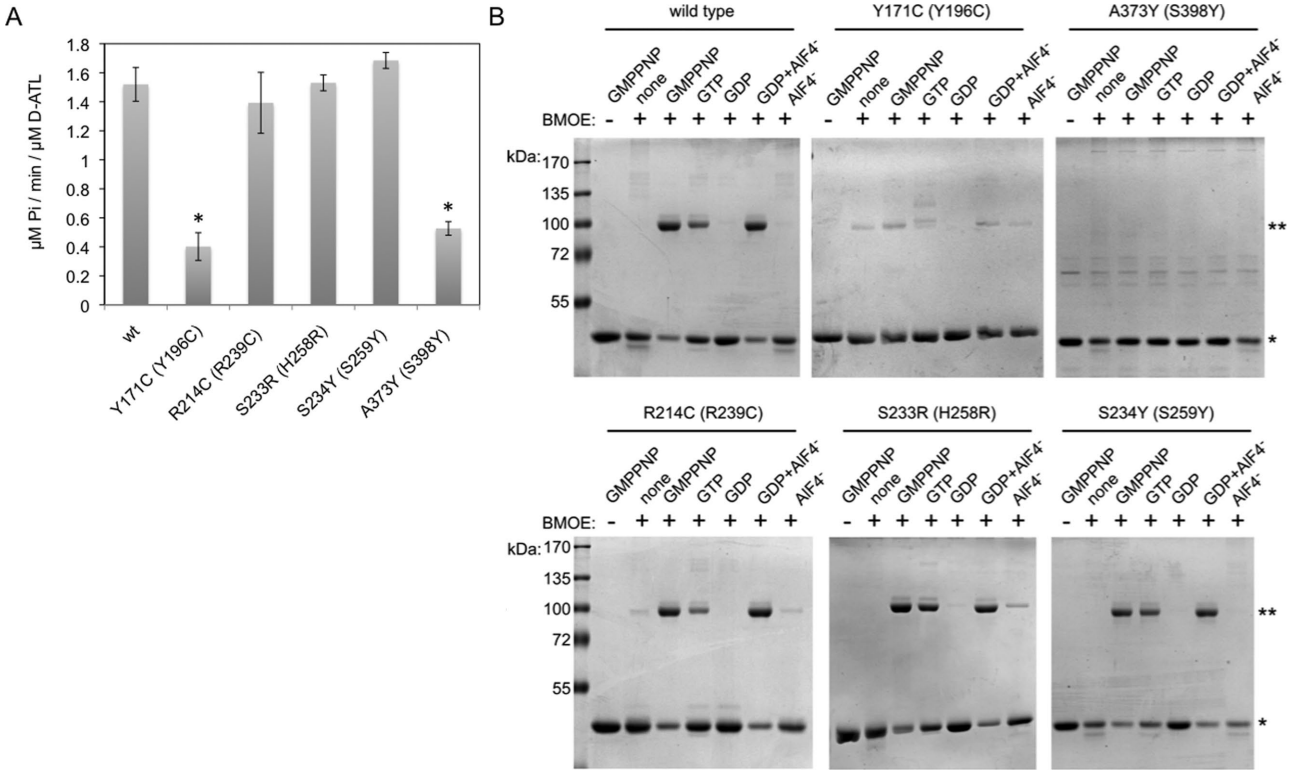

FIGURE 6: GTP hydrolysis and crossover dimer formation capabilities of SPG3A variants in the context of the *Drosophila* atlastin soluble domain. (A) GTPase activity. Purified soluble domain versions of *Drosophila* atlastin (aa 1–415) with the indicated SPG3A-equivalent mutations were assayed for GTPase activity. Values represent the means of three independent measurements ± SD. *$p < 0.0001$ with respect to the wild type (unpaired Student's *t* test). All others were not significantly different from the wild type. (B) Crossover dimer formation. The same purified proteins (from A) were incubated at room temperature in the absence or presence of the indicated nucleotides and then subjected to BMOE cross-linking. The single asterisk marks the soluble-domain monomer, and the double asterisk marks the cross-linked dimer. Results shown are representative of at least two independent experiments for each variant. All variants also had the G343C substitution, which enabled crossover-specific sulfhydryl cross-linking by BMOE. For clarity, the corresponding SPG3A mutation is also indicated in parentheses.

the basis of this information, we speculate that the Y196C substitution hinders crossover dimer formation, which in turn inhibits fusion. Of note, a mutation in P342 has recently been identified in an HSP patient (Zhu *et al.*, 2014). Closer study of this and the other nonfunctional atlastin1/SPG3A variants may uncover new insights into the conformational dynamics of 3HB rotation and crossover.

Our discovery of disease mutations with no apparent effect on atlastin activity was a surprise. Two variants, R239C and H258R (R214C and S233R in *Drosophila*), showed no measurable deficit in the context of either atlastin1 or *Drosophila* atlastin or whether in the context of cells or pure protein assays. A third variant, S234Y (S259Y in atlastin1), had only a slight reduction in fusion activity. The apparent functionality of these variants was of note because the mutations they harbor correspond to the very mutations in the kindreds, ADHSP-P (S259Y), ADHSP-T (H258R), and ADHSP-S (R239C), originally analyzed toward the identification of SPG3A as atlastin1 (Zhao *et al.*, 2001). As mentioned, R239C is the most commonly occurring SPG3A mutation in patients, identified 10 times more frequently than the others and in unrelated families (Namekawa *et al.*, 2006). In each of the original families, the disease was tightly linked to the SPG3A locus, with LOD scores of 4.63, 5.59, and 2.28 for ADHSP-P, ADHSP-T, and ADSP-S, respectively (Zhao *et al.*, 2001). Many subsequently identified SPG3A alleles have been uncovered solely on the basis of sequencing the SPG3A gene in patients after exclusion of a mutation in SPG4/spastin, the other common autosomal dominant HSP locus (Muglia *et al.*, 2002; Abel *et al.*, 2004; Sauter *et al.*, 2004; Rainier *et al.*, 2006). Consequently, some of the latter cases could, in principle, be attributable to a secondary mutation outside of the SPG3A locus. This seems unlikely, however, for the originally characterized mutations (Zhao *et al.*, 2001).

The atlastin1 levels in the neurons of patients heterozygous for the R239C and H258R mutations are unknown; therefore we cannot rule out the possibility they might be low enough to cause a fusion defect. However, neither the R239C nor H258R protein was unstable upon expression in neuroblast-derived PC12 cells (Supplemental Figure S7, A and B). This is in agreement with the previously reported wild-type level of thermostability of these variants in the soluble phase (Byrnes and Sondermann, 2011). Loss of atlastin1 has been reported in the lymphocytes of adult patients heterozygous for the ΔN436 mutation, a deletion of a single amino acid from the 3HB (Meijer *et al.*, 2007), although, the atlastin1 level in patients' neurons was not examined. We speculate that the loss of protein observed in the lymphocytes may have occurred as a secondary long-term consequence of ER structural perturbation. Indeed, we observed strong dominant-negative ER perturbation on expression of the ΔN436 variant in pC12 cells (Supplemental Figure S7A), whereas the R239C and H258R variants did not perturb ER morphology in any cell type analyzed (Supplemental Figure S7A and Figure 3). Consequently, protein loss would not be predicted for the latter.

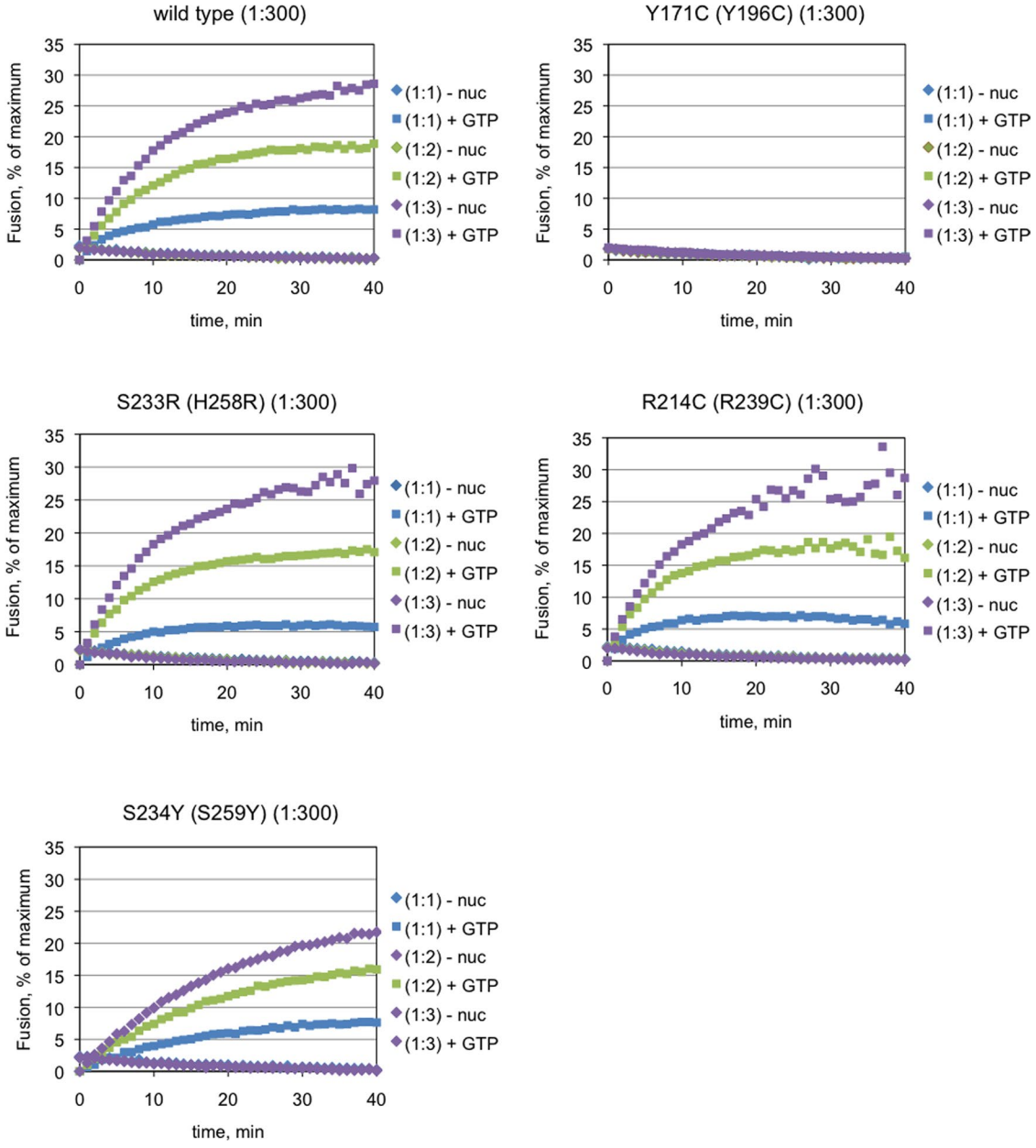

FIGURE 7: R214C, S233R, and S234Y but not Y171C *Drosophila* atlastin (R239C, H258R, and S259Y but not Y196C atlastin1) are fusion competent. Each of the indicated *Drosophila* atlastin variants was reconstituted into donor (labeled) and acceptor (unlabeled) vesicles at a 1:300 protein-to-lipid ratio. Fusion was monitored as the dequenching of fluorescent NBD-labeled lipid in donor vesicles after the addition of either GTP or buffer. For each variant, the reaction at three distinct donor-to-acceptor vesicle ratios is shown. The results shown are representative of at least two independent protein preparations.

The true effect of the R239C and H258R mutations on atlastin1 fusion activity remains unknown because the fusion assay in this study was carried out, by necessity, on *Drosophila* atlastin. Of interest, the histidine at position 258 in atlastin1, although highly conserved in vertebrate atlastins, is replaced by a serine and arginine in the *Drosophila* and *C. elegans* orthologues, respectively. The lack of conservation across the vertebrate/invertebrate divide may, in and of itself, argue against the residue serving an evolutionarily conserved core fusion function. Moreover, the H258R disease mutation converts the histidine to a residue already present in the *C. elegans* orthologue. Thus the H258R mutation would not have been predicted, a priori, to impair fusion. In contrast, R239 is at the dimer interface and conserved across all atlastin orthologues and is thus expected to serve a conserved and essential function. Still, we found no impairment in fusion or in any other biochemically assayable activity for the R239C variant. Despite the potential caveats pertaining to the use of the *Drosophila* orthologue, it is remarkable that no impairment could be discerned, at least within the confines of our assay conditions, for two of the three most prominent SPG3A disease variants. It might be argued that a slight reduction in fusion activity, within the margin of error in our assays, is sufficient to cause disease. A counterargument, however, is that the majority of atlastin1/SPG3A mutations are autosomal dominant, causing disease even in the presence of a wild-type copy of the gene (Zhao *et al.*, 2001). It is difficult to envision a

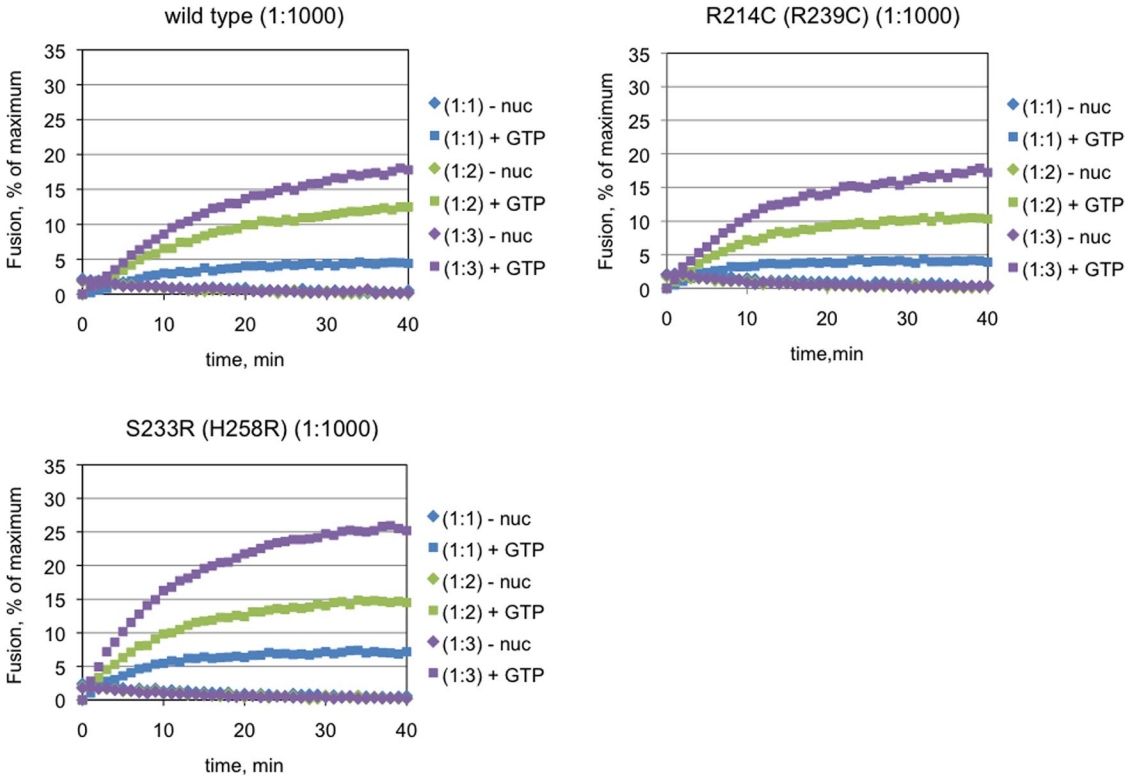

FIGURE 8: R214C and S233R *Drosophila* atlastin (R239C and H258R atlastin1) are similar to the wild type in their fusion activity. Each of the indicated *Drosophila* atlastin variants was reconstituted into donor (labeled) and acceptor (unlabeled) vesicles at a 1:1000 protein-to-lipid ratio. Fusion was monitored as the dequenching of fluorescent NBD-labeled lipid in donor vesicles after the addition of either GTP or buffer. For each variant, the reaction at three distinct donor-to-acceptor vesicle ratios is shown. The results shown are representative of at least two independent protein preparations.

scenario in which disease is caused by a slight, difficult- to-detect, reduction in the fusion activity in one of two atlastin1 alleles. Collectively our findings question the idea that SPG3A mutations cause HSP solely by disrupting the minimal machinery that catalyzes membrane fusion and ER morphogenesis.

Why then do these mutations cause disease? One possible explanation is that the ER in neurons is specialized and therefore relies on a neuron-specific factor that binds and regulates the fusion activity of atlastin1. In this case, R239 and H258, both surface exposed on the monomer, might constitute a binding interface for such a regulator. Another plausible explanation is that atlastin1 carries out an alternate, non-ER fusion function in neurons, and this alternate function is perturbed by the R239C and H258R mutations. In this context, it is noteworthy that atlastin1 has separately been implicated in bone morphogenetic protein (BMP) signaling (Fassier *et al.*, 2010). In the zebrafish, *Danio rerio*, atlastin1 knockdown caused severe larval mobility defects accompanied by alterations in spinal motor neuron architecture and a reduction in BMP receptor endocytosis (Fassier *et al.*, 2010). Remarkably, the mobility defects were rescued with an inhibitor of BMP signaling, suggesting that atlastin1 may normally down-regulate the BMP signaling pathway in neurons by directly or indirectly modulating BMP receptor internalization. Furthermore, spinal neurons isolated from atlastin1 morphants lacking atlastin1 and possibly relying on atlastin3 for ER membrane fusion (Rismanchi *et al.*, 2008) were reported to have normal ER morphology, implying that the mobility defects might not stem from ER morphological perturbations. On the other hand, the imaging methods used would not necessarily have enabled detection of branch-point density changes (Fassier *et al.*, 2010).

In sum, a significant level of uncertainty remains pertaining to the precise cellular role(s) of neuronal atlastin1. Although the behavior of some of the atlastin1/SPG3A variants analyzed here remains consistent with loss of ER membrane fusion as the root cause of HSP, the behavior of at least two disease variants is at odds with this hypothesis. The role and regulation of atlastin1 in the maintenance of long axons of the corticospinal tract may be complex, involving interplay among ER remodeling, microtubule interactions, receptor endocytosis, and signaling. Further investigation of the cellular role, mechanism, and regulation of atlastin1 in neurons is necessary to better understand the pathophysiology of SPG3A mutations.

MATERIALS AND METHODS

Cell culture, constructs, transfections, and reagents

HeLa and Cos-7 cells were maintained in MEM (Sigma-Aldrich, St. Louis, MO) and DMEM (Sigma-Aldrich), respectively, containing 10% fetal bovine serum (Atlanta Biologicals, Atlanta, GA) and 1% penicillin/streptomycin (Thermo Fisher Scientific, Waltham, MA) at 37°C in a 5% CO_2 incubator. PC12 cells were maintained on collagen IV (Sigma-Aldrich)–coated plates in F12K medium (Sigma-Aldrich) supplemented with 10% fetal bovine serum and 5% horse serum (Atlanta Biologicals). Transient plasmid DNA transfection of HeLa cells was performed using 1 µg of DNA and 2 µl of jetPEI (Polyplus, New York, NY) per 1 ml of medium according to the manufacturer's protocol. Cos-7 cell transfections were performed using 200 ng of DNA and 1.5 µl of Lipofectamine 2000 (Life Technologies, Grand Island, NY) per 0.5 ml of media, and PC12 transfections were performed using 1 µg of DNA and 7.5 µl of Lipofectamine in 1.5 ml of OptiMEM (Life Technologies). Atlastin2/3 siRNA transfections,

using atlastin2 (#1) and atlastin3 (#2) siRNAs identical in sequence to those previously published (Rismanchi *et al.*, 2008), were performed using 20 pmol of siRNA (10 pmol of each) and 2 µl of Oligofectamine (Life Technologies) in 0.5 ml of medium. eYFP-tagged *D. melanogaster* atlastin (Faust *et al.*, 2015), the hexahistidine (6xHis)-tagged, full-length *Drosophila* atlastin (Saini *et al.*, 2014), and the 6xHis-tagged soluble domain of *Drosophila* atlastin encoding aa 1–415 have been described previously (Saini *et al.*, 2014). The N-terminally HA-tagged atlastin1 was constructed by substituting the atlastin2 coding sequence in HA-tagged atlastin2 within *Xba*I and *Eco*RI sites (Morin-Leisk *et al.*, 2011) with a PCR-amplified fragment encoding aa 1–558 of atlastin1. The REEP1-Flag construct was generated by inserting the coding sequence of human REEP1 into the *Bam*HI and *Cla*I sites of the Cs2+MT vector. Subsequently, the Myc tag at the C-terminus was replaced with the Flag epitope (DYKDDDDK) following a short linker sequence (HRFKA). The Myc-REEP5/DP1/TB2 construct was previously described (Morin-Leisk *et al.*, 2011). All point mutations were generated using QuikChange Site-Directed Mutagenesis PCR (Qiagen, Valencia, CA) and fully verified by sequencing (Genewiz, South Plainfield, NJ). All lipids were purchased (Avanti Polar Lipids, Alabaster, AL). GTP, GDP, and GMPPNP were purchased (Sigma-Aldrich), reconstituted to 100 mM stocks in 10 mM Tris/1 mM EDTA, pH 8.0, and stored at −80°C. Antibodies used include a mouse monoclonal antibody (mAb) against the HA epitope (Sigma-Aldrich); the 9E10 mAb against the Myc epitope (gift from A. Linstedt, Carnegie Mellon University, Pittsburgh, PA); a Flag epitope mAb (Sigma-Aldrich); a polyclonal antibody (pAb) against calnexin (Abcam, Cambridge, MA); a pAb against REEP5 (Proteintech, Chicago, IL); and a pAb against tubulin (Abcam). Alexa 568–conjugated goat anti-mouse and fluorescein isothiocyanate–conjugated goat anti-rabbit secondary antibodies, as well as BODIPY 493/503, were purchased (Life Technologies).

Knockdown replacement assay

Cells plated on 60-mm dishes were transfected with 5 µg of the indicated HA-atlastin1 or eYFP-*Drosophila* atlastin constructs using transfection reagent jetPEI. Myc-tagged ER-resident protein REEP5/DP1/TB2, which did not affect either the percentage of cells showing the unbranched ER phenotype or the extent of loss of network branching relative to siRNA treatment alone (Morin-Leisk *et al.*, 2011), served as a negative control. At 24 h after DNA transfection, cells were trypsinized and replated onto 12-mm glass coverslips in a 24-well plate. siRNA treatment targeting both atlastin2 and atlastin3 was performed the next day. At 72 h after knockdown, cells were fixed in ice-cold methanol and processed for immunofluorescence (Morin-Leisk *et al.*, 2011). For quantification of functional replacement, the percentage of cells expressing the indicated HA-atlastin1 or eYFP-*Drosophila* atlastin that showed a loss of ER network branching (among ≥100 cells in three independent experiments) was determined. Nocodazole-washout experiments were performed as follows: 72 h after the second transfection (siRNA treatment), cells were incubated in 1 ml of medium containing 1 µg/ml nocodazole for 3 h, followed by washes with fresh medium without nocodazole. Cells were fixed at the indicated times after washout and processed for immunofluorescence (Morin-Leisk *et al.*, 2011).

Confocal microscopy

Cells were viewed using a spinning-disk confocal scanhead (Yokagawa; PerkinElmer, Akron, OH) mounted on an Axiovert 200 microscope (Zeiss, Thornwood, NY) with a 100×/1.4 numerical aperture (NA) objective (Zeiss) and acquired using a 16-bit ORCA-ER camera (Hamamatsu Photonics, Hamamatsu City, Japan). Maximal value projections of sections at 0.2-µm spacing were acquired using Micromanager open source software (University of California, San Francisco, San Francisco, CA) and imported as either 16- or 8-bit images in ImageJ open source software (National Institutes of Health, Bethesda, MD) or Photoshop (Adobe, San Jose, CA). For quantification of network branch points (Figure 1B), images of control or eYFP-*Drosophila* atlastin– or HA-atlastin1–expressing cells, acquired using identical acquisition parameters, were imported into ImageJ, where they were thresholded using a constant threshold value and skeletonized. The average number of three-way junctions in each of five 10 µm × 10 µm boxed peripheral regions was then manually counted. Quantification of functional replacement was performed manually on a wide-field Axioplan fluorescence microscope (Zeiss) with a 40×/1.4 NA objective.

REEP1 and atlastin1 co-redistribution assay

Cos-7 cells transfected with REEP1-Flag alone, eYFP-atlastin1 variants alone, or both were fixed and stained using the Flag antibody 48 h after transfection and viewed by confocal microscopy. To determine whether the large structures to which REEP1 and atlastin1 redistributed when coexpressed were lipid droplets, we cotransfected cells with REEP1-Flag and HA-atlastin1 variants, fixed them 48 h later, and costained them using either the Flag or HA antibody with BODIPY 493/503. The BODIPY 493/503 was dissolved in dimethyl sulfoxide at 1 mg/ml and added to the secondary antibody incubation at 1 µg/ml as previously described (Klemm *et al.*, 2013). Quantification of the number of large lipid droplet–like structures per cell was performed by importing confocal images, acquired as described, into ImageJ and obtaining a count of particles >0.7 µm in diameter after thresholding. We analyzed 5–10 fields/atlastin1 variant.

Measurement of protein stability in PC12 cells

Ten-centimeter dishes of PC12 cells were each transfected with 5 µg of HA-atlastin1 DNA and 30 µl of Lipofectamine 2000 in 10 ml OptiMEM. Transfection medium was replaced with growth medium after 4 h. At 24 h after transfection, cells on each dish were trypsinized and passed onto individual 3.5-cm dishes. Cycloheximide at a concentration of 0.1 mg/ml in growth medium, well documented to block protein synthesis (Gilden and Carp, 1966), was added 48 h after transfection for 0, 1, 2, or 4 h. Cells were harvested by scraping into ice-cold phosphate-buffered saline, collected by centrifugation at 6000 rpm for 5 min, resuspended in reducing sample buffer, resolved by SDS–PAGE, blotted onto nitrocellulose, and probed using antibodies against the HA epitope to detect HA-atlastin1 and antibodies to detect endogenous calnexin. Longer incubation times (6–8 h or longer) with cycloheximide led to cell death, as previously reported (Geier *et al.*, 1992).

Protein expression and purification

Full-length *Drosophila* atlastin protein expression was induced with 0.2 mM isopropyl-β-D-thiogalactoside (IPTG) in BL21(DE3)pLysS cells at 16°C for 2.5 h. Cells were lysed in 4% Triton X-100 (Roche, Basel, Switzerland) in a standard lysis buffer (50 mM Tris-HCl, pH 8.0, 5 mM $MgCl_2$, 500 mM NaCl, 10 mM imidazole, 10% glycerol, 2 mM 2-mercaptoethanol, 1 µg/ml leupeptin, and 1 µg/ml pepstatin) and 6xHis-tagged proteins purified using standard protocols on Ni^{2+} agarose beads (Qiagen). Bound protein was eluted in 50 mM Tris, pH 8.0, 250 mM imidazole, 100 mM NaCl, 5 mM $MgCl_2$, 10% glycerol, 2 mM 2-mercaptoethanol, 0.1% Anapoe-X 100 (Affymetrix, Santa Clara, CA), and 1 mM EDTA. Protein yields were typically 3–8 mg/ml (~1 mg/l of culture), >85% pure, flash frozen in liquid N_2,

and stored at −80°C. The 6xHis-tagged cytoplasmic domain of *Drosophila* atlastin protein expression was induced with 0.5 mM IPTG in BL21(DE3)pLysS cells at 20°C for 16 h and purified using standard protocols for purification of 6xHis-tagged proteins on Ni^{2+} agarose beads (Qiagen). Proteins eluted in 50 mM Tris, pH 8.0, 250 mM imidazole, 100 mM NaCl, 5 mM $MgCl_2$, and 10% glycerol were typically 10–24 mg/ml, >95% pure, flash frozen in liquid N_2, and stored at −80°C.

GTPase assay

Purified 6xHis-tagged *Drosophila* atlastin soluble domain (residues 1–415) and variant proteins were dialyzed into 50 mM Tris-HCl, pH 7.5, 100 mM NaCl, and 1 mM $MgCl_2$ at 4°C and precleared by centrifugation at 100,000 rpm (TLA100; Beckman, Indianapolis, IN) at 4°C for 15 min. GTPase activity was measured using the Enzchek Phosphate Assay Kit (Life Technologies). A standard reaction for GTPase measurements involved mixing 1 U/ml purine nucleoside phosphorylase and 0.2 mM 2-amino-6-mercapto-7-methylpurine riboside in the provided buffer (50 mM Tris-HCl, pH 7.5, 1 mM $MgCl_2$, 0.1 mM sodium azide) supplemented with 100 mM NaCl and 0.5 mM GTP in a total volume of 200 µl. After 10 min at 37°C, reactions were transferred to a 96-well plate (Costar, Washington, DC) and started by addition of either buffer or 6xHis-tagged *Drosophila* atlastin variants at a final concentration of 1 or 2 µM. Absorbance at 360 nm was monitored at 30-s intervals for 30 min at 37°C in a plate reader (Safire 2; Tecan, Mannedorf, Switzerland). Data were normalized to a phosphate standard and initial velocities calculated using the early linear portion of each curve.

Cross-linking

Purified 6xHis-tagged *Drosophila* atlastin soluble domain (residues 1–415) and variant proteins were dialyzed into SEC buffer (25 mM Tris-HCl, pH 7.0, 100 mM NaCl, 5 mM $MgCl_2$, 2 mM ethylene glycol tetraacetic acid) at 4°C and precleared by centrifugation at 100,000 rpm for 15 min (TLA100). We incubated 5 µM of each protein at room temperature in SEC buffer, pH 7.0, in the absence or presence of 2 mM GMPPNP, GDP, GTP, GDP-AlF_4^- (2 mM GDP/2 mM $AlCl_3$/20 mM NaF) or AlF_4^- only (2 mM $AlCl_3$/20 mM NaF). After 30 min at room temperature, the reaction was diluted 2.5-fold into SEC (to 2 µM D-ATL) in the absence or presence of 6 µM BMOE (Thermo Fisher Scientific) and incubated for 1 h at room temperature. Samples were then quenched with 20 mM dithiothreitol for 15 min, mixed with reducing sample buffer, resolved by SDS–PAGE, and stained with Coomassie blue.

Proteoliposome production

Lipids in chloroform dried down by rotary evaporation were hydrated by resuspension in A100 buffer (25 mM 4-(2-hydroxyethyl)-1-piperazineethanesulfonic acid, pH 7.4, 100 mM KCl, 10% glycerol, 2 mM β-mercaptoethanol, 1 mM EDTA; Moss *et al.*, 2011), final lipid concentration ~10 mM, and subjected to 12 freeze–thaw cycles in liquid N_2 and room temperature water. Liposomes of diameter 100–300 nm were formed by extrusion through 100-nm polycarbonate filters using the LipoFast LF-50 extruder (Avestin, Ottawa, ON, Canada). Unlabeled liposomes consisted of palmitoyloleoylphosphatidylcholine (POPC):dioleoyl phosphatidylserine (DOPS; 85:15), and labeled liposomes had POPC:DOPS:1,2-dipalmitoyl-*sn*-glycero-3-phosphoethanolamine-N-(7-nitro-2-1,3-benzoxadiazol-4-yl (DPPE-NBD):rhodamine-DPPE (82:15:1.5:1.5). *Drosophila* atlastin in 0.1% Anapoe-X 100 was reconstituted into preformed 100-nm liposomes as previously described (Moss *et al.*, 2011). In brief, reconstitutions were carried out at a protein-to-lipid ratio of 1:300 or 1:1000 at a constant lipid concentration and an effective detergent-to-lipid ratio of ~0.7 as previously described (Moss *et al.*, 2011). Protein and lipid were incubated at 4°C for 1 h. Detergent was removed by SM-2 Bio-Beads (Bio-Rad, Hercules, CA) at 70 mg of Triton X-100 per 1 g of beads. Insoluble protein aggregates were pelleted by centrifugation of the samples in a microcentrifuge for 10 min at 16,000 × *g*. Thereafter, reconstituted *Drosophila* atlastin proteoliposomes were adjusted to 50% Nycodenz and separated from unincorporated protein by flotation of proteoliposomes through a (50/45/0%) Nycodenz (Axis-Shield, Dundee, Scotland) 5-ml step gradient. All Nycodenz solutions were made in A100 buffer without glycerol. After centrifugation at 40,000 rpm for 16 h at 4°C in a SW-50.1 rotor, the gradient was fractionated and analyzed by SDS–PAGE stained with Coomassie blue to assess insertion efficiency (Supplemental Figures S3 and S4). The proteoliposomes typically migrated to the 45/0% Nycodenz interface. Finally, the floated fraction was desalted over a 2.4-ml Sephadex A (GE Healthcare, Piscataway, NJ) column into A100 buffer, stored at 4°C, and used within 72 h.

Fusion assay

Fusion assays were performed as previously described (Orso *et al.*, 2009; Moss *et al.*, 2011). Donor (0.2 mM) and acceptor proteoliposomes were mixed at molar ratios of 1:1, 1:2, and 1:3 in A100 buffer in the presence of 5 mM $MgCl_2$ in a total volume of 200 µl/reaction. The reaction mixture was transferred into a clear, flat-bottomed, polystyrene 96-well plate (Corning) and incubated at 37°C for 10 min. The fusion reaction was started by addition of 2 mM GTP (final concentration) or buffer. NBD fluorescence (excitation, 460 nm; emission, 538 nm) was measured at 1-min intervals with a 1-s shaking after every read. After 60 min, 10 µl of 10% Anapoe-X 100 was added to determine the total fluorescence in the sample. All measurements, reported as the percentage of total fluorescence after solubilization in Anapoe-X 100, were acquired on a Safire 2 fluorescence plate reader using Excel (Microsoft, Redmond, WA).

ACKNOWLEDGMENTS

James McNew (Rice University, Houston, TX) provided the GST-atlastin1 construct. The Molecular Biosensor Imaging Facility and B. Armitage and J. Minden (Carnegie Mellon University, Pittsburgh, PA) shared instruments essential for this study. J. Fink (University of Michigan, Ann Arbor, MI) provided helpful insights on the genetics of SPG3A. A. Linstedt gave helpful suggestions on the manuscript, and members of the Lee, Linstedt, and Puthenveedu labs (Carnegie Mellon University) offered suggestions throughout. This work was funded by a grant from the Spastic Paraplegia Foundation and Grants 1R21DK088208 and R01GM107285 from the National Institutes of Health to T.H.L.

REFERENCES

Abel A, Fonknechten N, Hofer A, Dürr A, Cruaud C, Voit T, Weissenbach J, Brice A, Klimpe S, Auburger G, Hazan J (2004). Early onset autosomal dominant spastic paraplegia caused by novel mutations in SPG3A. Neurogenetics 5, 239–243.

Anwar K, Klemm RW, Condon A, Severin KN, Zhang M, Ghirlando R, Hu J, Rapoport TA, Prinz WA (2012). The dynamin-like GTPase Sey1p mediates homotypic ER fusion in S. cerevisiae. J Cell Biol 197, 209–217.

Bian X, Klemm RW, Liu TY, Zhang M, Sun S, Sui X, Liu X, Rapoport TA, Hu J (2011). Structures of the atlastin GTPase provide insight into homotypic fusion of endoplasmic reticulum membranes. Proc Natl Acad Sci USA 108, 3976–3981.

Blackstone C (2012). Cellular pathways of hereditary spastic paraplegia. Annu Rev Neurosci 35, 25–47.

Blackstone C, O'Kane CJ, Reid E (2011). Hereditary spastic paraplegias: membrane traffic and the motor pathway. Nat Rev Neurosci 12, 31–42.
Byrnes LJ, Singh A, Szeto K, Benvin NM, O'Donnell JP, Zipfel WR, Sondermann H (2013). Structural basis for conformational switching and GTP loading of the large G protein atlastin. EMBO J 32, 369–384.
Byrnes LJ, Sondermann H (2011). Structural basis for the nucleotide-dependent dimerization of the large G protein atlastin-1/SPG3A. Proc Natl Acad Sci USA 108, 2216–2221.
Chappie JS, Acharya S, Leonard M, Schmid SL, Dyda F (2010). G domain dimerization controls dynamin's assembly-stimulated GTPase activity. Nature 465, 435–440.
Dailey ME, Bridgman PC (1989). Dynamics of the endoplasmic reticulum and other membranous organelles in growth cones of cultured neurons. J Neurosci 9, 1897–1909.
Daumke O, Praefcke GJ (2011). Structural insights into membrane fusion at the endoplasmic reticulum. Proc Natl Acad Sci USA 108, 2175–2176.
Deluca GC, Ebers GC, Esiri MM (2004). The extent of axonal loss in the long tracts in hereditary spastic paraplegia. Neuropathol Appl Neurobiol 30, 576–584.
Depienne C, Stevanin G, Brice A, Durr A (2007). Hereditary spastic paraplegias: an update. Curr Opin Neurol 20, 674–680.
Dreier L, Rapoport TA (2000). In vitro formation of the endoplasmic reticulum occurs independently of microtubules by a controlled fusion reaction. J Cell Biol 148, 883–898.
Fassier C, Hutt JA, Scholpp S, Lumsden A, Giros B, Nothias F, Schneider-Maunoury S, Houart C, Hazan J (2010). Zebrafish atlastin controls motility and spinal motor axon architecture via inhibition of the BMP pathway. Nat Neurosci 13, 1380–1387.
Faust JE, Desai T, Verma A, Ulengin I, Sun TL, Moss TJ, Betancourt MA, Huang HW, Lee T, McNew JA (2015). The atlastin C-terminal tail is an amphipathic helix that perturbs bilayer structure during endoplasmic reticulum homotypic fusion. J Biol Chem 290, 4772–4783.
Fink JK (2006). Hereditary spastic paraplegia. Curr Neurol Neurosci Rep 6, 65–76.
Friedman JR, Webster BM, Mastronarde DN, Verhey KJ, Voeltz GK (2010). ER sliding dynamics and ER-mitochondrial contacts occur on acetylated microtubules. J Cell Biol 190, 363–375.
Gasper R, Meyer S, Gotthardt K, Sirajuddin M, Wittinghofer A (2009). It takes two to tango: regulation of G proteins by dimerization. Nat Rev Mol Cell Biol 10, 423–429.
Geier A, Beery R, Haimshon M, Hemi R, Lunenfeld B (1992). Serum and insulin inhibit cell death induced by cycloheximide in the human breast cancer cell line MCF-7. In Vitro Cell Dev Biol 28A, 415–418.
Gilden RV, Carp RI (1966). Effects of cycloheximide and puromycin on synthesis of simian virus 40 T antigen in green monkey kidney cells. J Bacteriol 91, 1295–1297.
Gispert S, Santos N, Damen R, Voit T, Schulz J, Klockgether T, Orozco G, Kreuz F, Weissenbach J, Auburger G (1995). Autosomal dominant familial spastic paraplegia: reduction of the FSP1 candidate region on chromosome 14q to 7 cM and locus heterogeneity. Am J Hum Genet 56, 183–187.
Guelly C, Zhu PP, Leonardis L, Papić L, Zidar J, Schabhüttl M, Strohmaier H, Weis J, Strom TM, Baets J, *et al*. (2011). Targeted high-throughput sequencing identifies mutations in atlastin-1 as a cause of hereditary sensory neuropathy type I. Am J Hum Genet 88, 99–105.
Hashimoto Y, Shirane M, Matsuzaki F, Saita S, Ohnishi T, Nakayama KI (2014). Protrudin regulates endoplasmic reticulum morphology and function associated with the pathogenesis of hereditary spastic paraplegia. J Biol Chem 289, 12946–12961.
Hazan J, Lamy C, Melki J, Munnich A, de Recondo J, Weissenbach J (1993). Autosomal dominant familial spastic paraplegia is genetically heterogeneous and one locus maps to chromosome 14q. Nat Genet 5, 163–167.
Hu J, Shibata Y, Zhu PP, Voss C, Rismanchi N, Prinz WA, Rapoport TA, Blackstone C (2009). A class of dynamin-like GTPases involved in the generation of the tubular ER network. Cell 138, 549–561.
Klemm RW, Norton JP, Cole RA, Li CS, Park SH, Crane MM, Li L, Jin D, Boye-Doe A, Liu TY, *et al*. (2013). A conserved role for atlastin GTPases in regulating lipid droplet size. Cell Rep 3, 1465–1475.
Listenberger LL, Brown DA (2007). Fluorescent detection of lipid droplets and associated proteins. Curr Protoc Cell Biol Chapter 24, Unit 24.22.
Lo Giudice T, Lombardi F, Santorelli FM, Kawarai T, Orlacchio A (2014). Hereditary spastic paraplegia: clinical-genetic characteristics and evolving molecular mechanisms. Exp Neurol 261, 518–539.
Lu L, Ladinsky MS, Kirchhausen T (2009). Cisternal organization of the endoplasmic reticulum during mitosis. Mol Biol Cell 20, 3471–3480.
Meijer IA, Dion P, Laurent S, Dupré N, Brais B, Levert A, Puymirat J, Rioux MF, Sylvain M, Zhu PP, *et al*. (2007). Characterization of a novel SPG3A deletion in a French-Canadian family. Ann Neurol 61, 599–603.
Morin-Leisk J, Saini SG, Meng X, Makhov AM, Zhang P, Lee TH (2011). An intramolecular salt bridge drives the soluble domain of GTP-bound atlastin into the postfusion conformation. J Cell Biol 195, 605–615.
Moss TJ, Andreazza C, Verma A, Daga A, McNew JA (2011). Membrane fusion by the GTPase atlastin requires a conserved C-terminal cytoplasmic tail and dimerization through the middle domain. Proc Natl Acad Sci USA 108, 11133–11138.
Muglia M, Magariello A, Nicoletti G, Patitucci A, Gabriele AL, Conforti FL, Mazzei R, Caracciolo M, Casari G, Ardito B, *et al*. (2002). A large family with pure autosomal dominant hereditary spastic paraplegia from southern Italy mapping to chromosome 14q11.2-q24.3. J Neurol 249, 1413–1416.
Namekawa M, Ribai P, Nelson I, Forlani S, Fellmann F, Goizet C, Depienne C, Stevanin G, Ruberg M, Dürr A, Brice A (2006). SPG3A is the most frequent cause of hereditary spastic paraplegia with onset before age 10 years. Neurology 66, 112–114.
Orso G, Pendin D, Liu S, Tosetto J, Moss TJ, Faust JE, Micaroni M, Egorova A, Martinuzzi A, McNew JA, Daga A (2009). Homotypic fusion of ER membranes requires the dynamin-like GTPase atlastin. Nature 460, 978–983.
Park SH, Zhu PP, Parker RL, Blackstone C (2010). Hereditary spastic paraplegia proteins REEP1, spastin, and atlastin-1 coordinate microtubule interactions with the tubular ER network. J Clin Invest 120, 1097–1110.
Pendin D, Tosetto J, Moss TJ, Andreazza C, Moro S, McNew JA, Daga A (2011). GTP-dependent packing of a three-helix bundle is required for atlastin-mediated fusion. Proc Natl Acad Sci USA 108, 16283–16288.
Praefcke GJ, McMahon HT (2004). The dynamin superfamily: universal membrane tubulation and fission molecules? Nat Rev Mol Cell Biol 5, 133–147.
Rainier S, Hedera P, Alvarado D, Zhao X, Kleopa KA, Heiman-Patterson T, Fink JK (2001). Hereditary spastic paraplegia linked to chromosome 14q11-q21: reduction of the SPG3 locus interval from 5.3 to 2.7 cM. J Med Genet 38, E39.
Rainier S, Sher C, Reish O, Thomas D, Fink JK (2006). De novo occurrence of novel SPG3A/atlastin mutation presenting as cerebral palsy. Arch Neurol 63, 445–447.
Rismanchi N, Soderblom C, Stadler J, Zhu PP, Blackstone C (2008). Atlastin GTPases are required for Golgi apparatus and ER morphogenesis. Hum Mol Genet 17, 1591–1604.
Saini SG, Liu C, Zhang P, Lee TH (2014). Membrane tethering by the atlastin GTPase depends on GTP hydrolysis but not on forming the crossover configuration. Mol Biol Cell 25, 3942–3953.
Salinas S, Proukakis C, Crosby A, Warner TT (2008). Hereditary spastic paraplegia: clinical features and pathogenetic mechanisms. Lancet Neurol 7, 1127–1138.
Sauter SM, Engel W, Neumann LM, Kunze J, Neesen J (2004). Novel mutations in the Atlastin gene (SPG3A) in families with autosomal dominant hereditary spastic paraplegia and evidence for late onset forms of HSP linked to the SPG3A locus. Hum Mutat 23, 98.
Terasaki M, Chen LB, Fujiwara K (1986). Microtubules and the endoplasmic reticulum are highly interdependent structures. J Cell Biol 103, 1557–1568.
Terasaki M, Slater NT, Fein A, Schmidek A, Reese TS (1994). Continuous network of endoplasmic reticulum in cerebellar Purkinje neurons. Proc Natl Acad Sci USA 91, 7510–7514.
Waterman-Storer CM, Salmon ED (1998). Endoplasmic reticulum membrane tubules are distributed by microtubules in living cells using three distinct mechanisms. Curr Biol 8, 798–806.
Wu F, Hu X, Bian X, Liu X, Hu J (2015). Comparison of human and Drosophila atlastin GTPases. Protein Cell 6, 139–146.
Zhang M, Wu F, Shi J, Zhu Y, Zhu Z, Gong Q, Hu J (2013). ROOT HAIR DEFECTIVE3 family of dynamin-like GTPases mediates homotypic endoplasmic reticulum fusion and is essential for Arabidopsis development. Plant Physiol 163, 713–720.
Zhao X, Alvarado D, Rainier S, Lemons R, Hedera P, Weber CH, Tukel T, Apak M, Heiman-Patterson T, Ming L, *et al*. (2001). Mutations in a newly identified GTPase gene cause autosomal dominant hereditary spastic paraplegia. Nat Genet 29, 326–331.
Zhu PP, Denton KR, Pierson TM, Li XJ, Blackstone C (2014). Pharmacologic rescue of axon growth defects in a human iPSC model of hereditary spastic paraplegia SPG3A. Hum Mol Genet 23, 5638–48.
Zhu PP, Soderblom C, Tao-Cheng JH, Stadler J, Blackstone C (2006). SPG3A protein atlastin-1 is enriched in growth cones and promotes axon elongation during neuronal development. Hum Mol Genet 15, 1343–1353.